Chemical Engineering Journal 401 (2020) 126102

Contents lists available at ScienceDirect

Chemical Engineering Journal

journal homepage: www.elsevier.com/locate/cej

A novel removal strategy for copper and arsenic by photooxidation coupled with coprecipitation: Performance and mechanism

Wei Ding[a,b], Hui Tong[c,d], Dan Zhao[b], Huaili Zheng[a], Chengshuai Liu[c,d,*], Jinjun Li[b], Feng Wu[b,*]

[a] College of Environment and Ecology, Chongqing University, Chongqing 400044, PR China
[b] School of Resources and Environmental Science, Wuhan University, Wuhan 430079, PR China
[c] State Key Laboratory of Environmental Geochemistry, Institute of Geochemistry, Chinese Academy of Sciences, Guiyang 550081, PR China
[d] Guangdong Key Laboratory of Agro-environmental Pollution Control and Management, Guangdong Institute of Eco-environmental Science & Technology, Guangzhou 510650, PR China

HIGHLIGHTS

- A photo-enhanced removal of As(III) and Cu(II) was achieved.
- As(III) removal was through a combination of photooxidation and coprecipitation.
- As(III) photooxidation relied on the formation of the Cu(II)–As(III) complex.
- As(III) complexed with Cu(II) is photooxidized via direct electron transfer.
- Procedures to realize the light-enhanced water's purification were proposed.

GRAPHICAL ABSTRACT

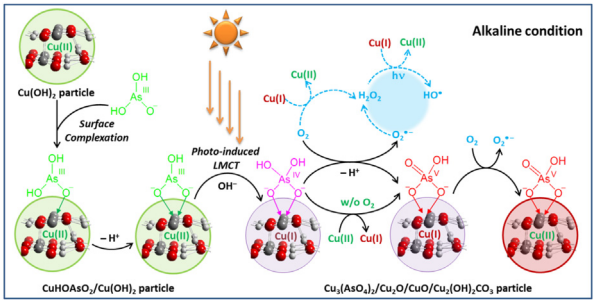

ARTICLE INFO

Keywords:
Copper/arsenic contamination
Surface complexation
Solar radiation
Photooxidation
Direct electron transfer

ABSTRACT

Arsenic and copper causing water pollution is a worldwide problem, and simultaneously achieving water decontamination from arsenic and copper is immensely attractive. In this study, an economical and eco-friendly light-enhanced removal system was proposed to simultaneously alleviate water contamination from arsenic and copper, where nascent copper hydroxides (CHO) acted as nano-absorbers and electron acceptors for As(III) removal. According to the mechanism studies, the nascent CHO effectively capture As(III) forming surface Cu (II)–As(III) complex (formation constant, log K_{f1} = 6.0). Then, light induced the ligand-to-metal charge transfer (LMCT) from As(III) to Cu(II) inside the Cu(II)–As(III) complex, thus leading to both As(III) oxidation and Cu(II) reduction under anoxic conditions. The quantum yield of As(III) photooxidation at 365 nm was ascertained as $(2.3 \pm 0.2) \times 10^{-2}$. The final photoproducts can be easily recycled as stabilized Cu(II)–As(V) complex and deposit. Real sunlight-driven photooxidation of As(III) in the presence of CHO and As(III) photooxidation to As (V) in solid Cu(II)–As(III) complex were also confirmed, which implying the promising application in practical water treatment. Accordingly, the oxygen-independent and light-enhanced removal of arsenic and copper can help develop recovery strategies for copper and arsenic.

* Corresponding authors at: State Key Laboratory of Environmental Geochemistry, Institute of Geochemistry, Chinese Academy of Sciences, Guiyang 550081, PR China (C. Liu); School of Resources and Environmental Science, Wuhan University, Wuhan 430079, PR China (F. Wu).
E-mail addresses: liuchengshuai@vip.gyig.ac.cn (C. Liu), fengwu@whu.edu.cn (F. Wu).

https://doi.org/10.1016/j.cej.2020.126102
Received 15 May 2020; Received in revised form 24 June 2020; Accepted 26 June 2020
Available online 01 July 2020
1385-8947/

1. Introduction

Arsenic has aroused a global attention for its carcinogenicity and toxicity to humans and usually enters human bodies via water [1,2]. Arsenic is usually released into water source in two primary inorganic forms, i.e., arsenite species (As(III)) and arsenate species (As(V)) through natural processes or anthropogenic activities [3]. For instance, arsenic is usually produced as a by-product of base metals smelting, in particular copper, lead, cobalt and nickel concentrates [4]. Thus a complex industrial wastewater is produced during the smelting of nonferrous metal sulfide ores containing high concentrations of arsenic and heavy metals [5]. Currently, the increased consumption of low-grade sulfide ores with high arsenic content are exploited in smelting plants due to the growing mineral resource shortage, which increases arsenic levels in the wastewater (3–10 $g{\cdot}L^{-1}$) [6,7]. In these produced wastewater, arsenic mainly exists as As(III) compounds (arsenious acid) [5], which is significantly more toxic and mobile than As(V) [8]. The long-term exposure to the high level of inorganic arsenic has led to emergency public health incidents [9]. Thus treatment of As(III) contaminated water is imperative before intake.

The reliable and efficient approaches to mitigate water pollution could be divided into two broad classes: separation [10,11] and degradation [12–16]. Unsurprisingly, given that the degradation of As(III) is theoretically impossible, diverse separation approaches for removing arsenic have been developed [17]. For instance, precipitation is successfully tested in laboratory and widely applied in industrial scale. After the addition of lime or ferric salts and the up-regulation of pH, the arsenic is removed from the wastewater by forming the precipitate with calcium or iron [18,19]. However, the precipitation treatment usually produces a large amount of unstable arsenic-bearing sludge, which potentially cases secondary pollutions during long-term storage [20]. Adsorption is considered as an efficient and economic method for water decontamination from arsenic [21,22]. Several reports showed that Cu (II) oxides can adsorb As(V)/As(III) efficiently due to its high surface area and high point of zero charge [23–29]. In alkaline solution, Goswami et al. [24] found that As(III) adsorption on the Cu(II) oxide surface was more efficient compared with that at an acid pH. Previous study has shown arsenic strongly binding to Cu(II) oxides primarily through inner-sphere complexation structures [29]. Herein, Cu(II) oxides based materials are viewed as efficient absorbents for arsenic removal under alkaline condition. Fortunately for some though, copper usually coexists in the arsenic containing industrial wastewater because arsenic is often contained within tennantite (51.6% Cu and 20.3% As) or enargite (48.4% Cu and 19.1% As), as copper ores for copper smelting [30]. The copper contaminated water also poses a severe threat and damage to local environments and humans and even causes various diseases [31]. The nascent Cu(II) (hydr)oxides (CHO) generated via the hydrolysis of Cu(II) can capture As(V)/As(III) oxyanions forming complexes in alkaline environments [32]. Inspired by those, the simultaneous removal of arsenic and copper seems to be achieved in alkaline condition.

In the abovementioned separation methods, most of arsenic is removed at the unoxidized state (As(III)), thus its high toxicity is not effectively reduced. Besides, arsenic removal by Cu(II) oxides depends on the oxidation state of arsenic species [24]. Hence, oxidation of As (III) to As(V) is regarded as a necessary strategy for effective arsenic removal, causing added complexity. Based on the results of the high-resolution X-ray photoelectron spectroscopy (XPS) of the As3d peaks, researchers found that adsorbed As(III) can occasionally be oxidized on the surfaces of Cu(II) oxides, whether natural or synthesized copper-arsenic minerals [26–29,33]. This might be attributed to the high-energy X-ray-driven potential electron transfer from As(III) to metal cations [34,35]. However, the mechanism of As(III) oxidation during As (III) removal by Cu(II) oxides has not been addressed in literature in a sophisticated manner.

According to previous works, rapid oxidation of As(III) was observed following its surface complexation with nascent colloid ferric hydroxide (CFH) in simulated sunlight [36]. The ligand-to-metal charge transfer (LMCT) from the As(III) anion to the Fe(III) cation, instead of any reactive oxygen species (ROS), was verified to account for As(III) oxidation. In fact, the environmental photochemistry of carboxylate complexes with Cu(II) is similar to that of Fe(III) [37,38]. Furthermore, the Cu(I) complex and an oxidized ligand radical are consequently produced through the photolysis of Cu(II) complexes with dicarboxylates [39,40], amino acids [41], iminodiacetic acid [42], nitrilotriacetic acid [43], and dissolved organic matters (DOMs) [44] upon irradiation of LMCT bands in the UV–vis region, and can be further oxidized. Inspired by those, As(III) may form a surface complex with CHO, and it is reasonable that As(III) can be oxidized in the same manner of LMCT as its surface complex occurs on CFH in sunlight. Furthermore, the produced copper arsenate precipitate possesses higher stabilization than arsenic compounds and can be easily separated from other copper precipitates (e.g., $Cu(OH)_2$ or $Cu_2(OH)_2CO_3$) by settling rates. Therefore, the light-induced removal of As(III) and Cu(II) can be reviewed as a potential strategy for remediation of polluted water under the iron-free condition.

In this work, we focused on identification and chemical description of mechanisms governing light-induced oxidation of As(III) during As (III) removal by nascent CHO under oxic and anoxic conditions. The specific aims of this study were (i) to verify the performance of the light-enhanced As(III) removal by nascent CHO; (ii) to confirm the importance of surface complexation between As(III) and CHO for As(III) oxidation and removal; (iii) to illustrate the photochemical reactions between As(III) and Cu(II) through LMCT within the complexes on CHO surface. The results may help to provide a novel strategy for the recovery of copper and arsenic from wastewater.

2. Materials and methods

2.1. Chemicals

All chemicals are of analytical grade and used without being further purified. The details of chemicals are presented in Text S1 in Supporting Information (SI).

2.2. Preparation and formation of a solid Cu(II)–As(III) complex

The solid Cu(II)–As(III) product was prepared by dissolving $CuSO_4$ in a specific amount in alkaline As(III) solution (Cu(II)/As(III)/NaOH molar ratio 1:2:4), and then the solution was adjusted to pH 10 using H_2SO_4. The mixture was further stirred at 20 °C for 6 h, and some green precipitate was formed, separated by a 0.22-μm filter, washed with ultrapure water three times, and then dried in an oven at 60 °C overnight. The characterization methodology is illustrated in Text S2.

2.3. Photochemical transformation experiments

Batch irradiation experiments were performed in a 750 mL water-jacketed vessel. A 500 mL reaction solution containing 200 μM Cu(II) and 5 μM As(III) was placed in the vessel exposed to the atmosphere. A control experiment was conducted in the dark by covering the vessel with aluminum-foil. Ten 8-W black light lamps (Phillips TLD-8 W, NL) that emitted UV-A light with λ_{max} of 365 nm (Fig. S1) were placed around the vessel (Fig. S2). The average irradiation intensity on the surface suspensions in the reactor was approximately 0.2 mW cm^{-2}, ascertained by a digital irradiance meter (SM206, Shenzhen Sanpometer Ltd., Shenzhen, China). The lamps were pre-switched for 20 min before the reaction to achieve stable irradiation intensity. The reaction temperature was maintained at 25 °C, and the premeditated pH was adjusted using 2 M NaOH solution. Subsequently, the reaction vessel was placed into the reactor to initialize the reaction. Samples were taken out from the reactor at certain time intervals, and preserved in

HCl (1:1 v/v) solution for further analysis unless noted otherwise.

In solar experiments, the real sun replaced black light lamps as the light resource, and all other procedures were the same as in above batch experiments. The solar experiments were conducted at different times during a day in summer in order to simulate different light intensities.

Aeration experiments under the irradiation of black light lamps were conducted in same reaction vessel with a rubber seal, and the solutions containing 200 μM Cu(II) and 5 μM As(III) were purged with compressed air (20.8% v/v O_2 and 79.2% v/v N_2 without CO_2) or N_2 (99.99%) for at least 30 min before and during the overall photoreaction. The dissolved oxygen content of each solution was determined by a dissolved oxygen meter (8403, AZ Instrument Co. Ltd.). During anoxic reaction, the content of dissolved oxygen was < 0.01 mg L^{-1} all the time.

In arsenic adsorption experiments, samples were taken and centrifuged for 7 min at 12000 rpm. The supernatant was acidized and used to determine the aqueous arsenic in solution.

To investigate the aggregation effect of CHO on As(III) photooxidation over time under alkaline conditions, the nascent CHO was aged for 2 h at pH 10. The changes in the particle size of CHO over time were monitored, and the aged CHO was used for As(III) photooxidation.

Prior to conducting the photolysis experiment of the solid Cu(II)–As(III) complex at pH 10, 10 mg L^{-1} of the solid Cu(II)–As(III) complex was dispersed in 500 mL water by an ultrasonic machine (JT820HTD, JATO Instrument Co. Ltd., Shenzhen, China) for 1 h before irradiation.

All experiments were performed in triplicate and average values are presented. The corresponding error bars are presented in each figure.

2.4. Analysis methods

Withdrawn samples were preserved in HCl (1:1 v/v) solution, and the acidic conditions was adopted to dissolve arsenic species and Cu(II/I) (hydr)oxides and to stabilize Cu(I) ions in N_2 atmosphere. As(III) and As(V) concentrations were analyzed based on our previous work [45]. The concentration of As(III) and As(V) were further determined on a liquid chromatography-hydride generation-atomic fluorescence spectrometry (LC-HG-AFS, Bohui Innovation Technology Co. Ltd., Beijing, China). The determination of Cu(I) concentration was conducted with a modified bathocuproine method [46]. In brief, the Cu(I) concentrations were analyzed by adding the chelating agent bathocuproine in water baths at 25 °C for 10 min and then the absorbance was recorded on a spectrophotometry at 484 nm (Shimadzu UV-1601, Kyoto, Japan). H_2O_2 concentration was ascertained using DPD photometric method at a wavelength of 551 nm [47]. The pH metric titrations method proposed by Bjerrum [48] and modified by Irving and Rossotti [49] was applied to determine the formation constants of Cu(II)–As(III) complex. The details of analyses are described in Text S3.

The distribution of Cu(II) species with or without tiron and the concentration of As(III) oxyanion ($AsO(OH)_2^-$) versus pH were simulated using Medusa software supported by KTH Royal Institute of Technology (Sweden).

The spectra of the solutions containing Cu(II) and/or As(III) were recorded on the Shimadzu UV-1601 spectrophotometer using a 1 cm cell. To ensure the reaction solution at pH < 3 before pH adjustment, Cu(II) stock solution was acidized by H_2SO_4. The pH was adjusted to 10 in 2 min with 2 M NaOH solution, and the reaction solution was stirred in dark at 25 °C for 1 h before UV–vis spectrum scanning.

3. Results and discussion

3.1. Photochemical transformation of As(III) in Cu(II) solutions at various pH

Batch irradiation experiments were conducted to investigate the effect of pH on As(III) photooxidation in 200 μM Cu(II)-contained solutions at pH 3–10, and the results are shown in Fig. 1a. The control

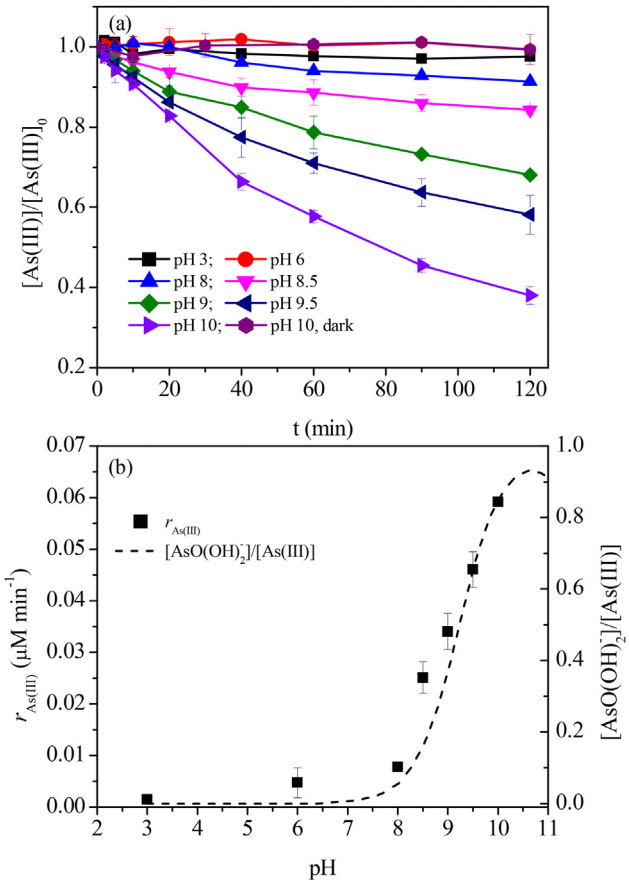

Fig. 1. (a) Variations of As(III) concentrations and (b) variations of the initial oxidation rate of As(III) ($r_{As(III)}$) and $AsO(OH)_2^-$ concentration fraction over pH range 3–10. Conditions: [Cu(II)] = 200 μM, [As(III)] = 5 μM, T = 25 °C.

experiments in dark exhibited no distinct As(III) oxidation at pH 3–10 within 120 min (data not all displayed), whereas a drop in As(III) concentration occurred within 120 min at pH 10 under UV-A irradiation. The mass balance of arsenic species during photochemical reaction in the solution at pH 10 demonstrated that the drop in As(III) concentration was attributed to photooxidation (Fig. S3). As(III) oxidation was limited under acidic or near neutral conditions (e.g. pH 3 or 6), whereas the oxidation efficiency of As(III) was enhanced from 8.7% to 62.0% when the initial pH increased from 8 to 10.

Compared with acidic condition, the alkaline condition benefited the adsorption of As(III) on copper (hydro)oxides [24]. Considering the Cu(II) species distribution in the absence of As(III) (Fig. S4), Cu(II) existed primarily as free Cu^{2+} under acidic conditions, exhibiting no photochemical activity for As(III) oxidation (Fig. 1a) because no obvious absorption at 365 nm was observed in the UV–vis spectra of the Cu(II)–As(III) solution (200 μM Cu(II) and 5 μM As(III)) at pH 3 (Fig. S5). After the CHO formation, the oxidation of As(III) occurred and increased under UV-A irradiation as pH increased from 8 to 10. These results indicated the dependence of As(III) oxidation on the formation of CHO in alkaline solutions under lighting conditions. Besides, negative $AsO(OH)_2^-$ oxyanion, as the dominant As(III) species under alkaline conditions, possessed a lower redox potential and a higher affinity to copper (hydr)oxides compared with $As(OH)_3$ [24]. This suggested that $AsO(OH)_2^-$ oxyanion, relative to $As(OH)_3$, may be easier to react with CHO which was formed at pH > 6. The close consistence between the initial rates of As(III) oxidation ($r_{As(III)}$) and the increasing concentration ratio of $AsO(OH)_2^-$ is observed in Fig. 1b, suggesting that As(III) photooxidation might rely on both the formation of CHO and $AsO(OH)_2^-$. Thus, the reaction could be terminated by acidifying the

samples. In the present study, HCl (1:1 v/v) was used to terminate the reaction and dissociate Cu(II)–As(III)/As(V) complexes for As(V)/As (III) analysis.

It is noteworthy that the pH dropped from 10 to 9.3 in the reactor opened to air throughout As(III) photooxidation, whereas no obvious variation in pH was observed in compressed air bubbling experiments (Fig. S6a). However, the As(III) oxidation in the compressed air bubbling experiment was similar to that exposed to air (Fig. S6b). These results revealed that the CO_2 dissolution from air to the solution accounted for pH decrease, and the slight effect on As(III) oxidation was probably attributed to the low concentration (ca. 78.7 μM) of H_2CO_3 calculated using the dissociation constants ($pK_{a1,2}$ = 6.35, 10.33). As shown in Fig. S6b, the addition of 100 μM $NaHCO_3$ didn't affect As(III) oxidation obviously, whereas < 10% of As(III) oxidation was observed when CHO was replaced by $Cu_2(OH)_2CO_3$ as Cu(II) source. Accordingly, As(III) photooxidation may occur after its quick adsorption/complexation on CHO under alkaline conditions, and the following experiments were performed in the reactor open to air unless noted otherwise.

3.2. Effects of HO˙ quencher and competitive ligand on As(III) photooxidation

Free radicals (i.e. $O_2^{\cdot -}$ and HO˙) and H_2O_2 are generally the dominant agents leading to oxidation of As(III) in photochemical reactions [36,50]. As a reductant under alkaline conditions, $O_2^{\cdot -}$ cannot oxidize As(III). During the photooxidation of As(III) at pH 10, almost no H_2O_2 (< 0.01 μM) was detected (Fig. S7), and H_2O_2 at such a low concentration cannot oxidize As(III) either [45]. Thus, we investigated the effect of HO˙ quencher on As(III) photooxidation. Ethanol acted as HO˙ probe with the rate constant of $k_{HO/ethanol}$ = (1.2–2.8) × 10^9 M^{-1} s^{-1} at 25 °C [51], close to that between As(III) and HO˙ ($k_{HO/As(III)}$ = (8.5–9.0) × 10^9 M^{-1} s^{-1}) at room temperature [36]. Thus, ethanol at concentration of 20-fold As(III) should be sufficient high to inhibit As (III) oxidation if HO˙ was responsible for As(III) oxidation. According to the results in Fig. 2, even the concentration of ethanol was 100-fold that of As(III), As(III) oxidation was not observably inhibited, which indicated that CHO didn't generate sufficient HO˙ that being responsible for As(III) photooxidation under UV-A irradiation.

The previous report demonstrated that As(III) could be adsorbed onto nascent colloidal ferric hydroxide by forming a surface complex at pH > 6 [36]. Thus, we proposed a hypothesis that As(III) photooxidation may occur through a ligand-to-metal charge-transfer (LMCT) process between As(III) and Cu(II) after their quick adsorption/complexation on CHO under alkaline conditions. The adsorption/

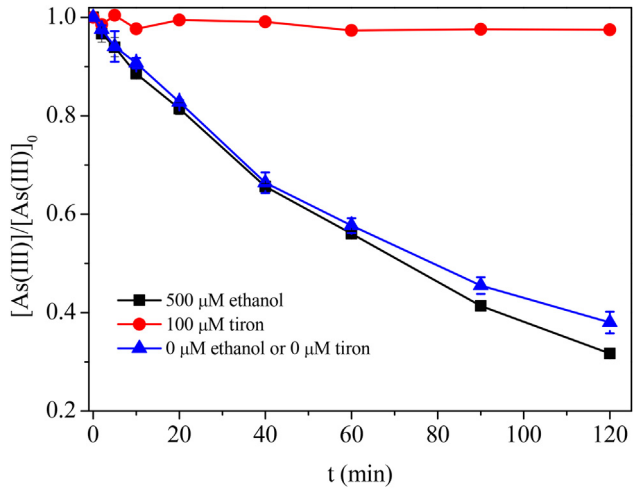

Fig. 2. Effects of ethanol and tiron on As(III) photooxidation. Conditions: [Cu (II)] = 200 μM, [As(III)] = 5 μM, [ethanol] = 500 μM, [tiron] = 100 μM, pH 10, T = 25 °C.

complexation between As(III) and CHO is the prerequisite for LMCT process and partly changes the morphology of CHO. Tiron was used as the competitive ligand for As(III) since it is very soluble in water and has an appropriate structure for complexation with Cu(II) [52]. The formation constants of Cu(II)–tiron complexes are 12.76 (log K_1) and 23.73 (log K_2), greater than those of Cu(II)–OH complexes (log $K_{1\text{-}4}$ = 7.0, 13.68, 17.00 and 18.5, respectively). The photooxidation of 5 μM As(III) was fully inhibited by 100 μM tiron (Fig. 2). In fact, 100 μM tiron can partially affect the formation CHO, and ~ 80% of Cu(II) remained in the form of CHO in the absence of As(III) at pH 10 (Fig. S8). This result suggested that (i) tiron competed with As(III) in complexation with Cu(II) on CHO surface and interrupted the interaction between As(III) and Cu(II); (ii) As(III) oxidation was not attributed to the photochemical activity of CHO itself, since the rest of CHO (80%) in the presence of tiron induced no As(III) oxidation at all. Therefore, As(III) photooxidation might occur via LMCT between As(III) and Cu(II) after the formation of As(III)–CHO complex.

3.3. LMCT process between As(III) and Cu(II)

In the LMCT process, the electron should be transformed from As (III) to Cu(II) on CHO surface along with As(III) oxidation to As(V). Thus, the oxygen would be dispensable for As(III) oxidation. Herein, comparison of As(III) photooxidation under oxic (open to air) or anoxic (N_2 bubbling) conditions was studied and the results are shown in Fig. 3a. Under anoxic conditions, 50.0% of As(III) photooxidation was still observed after 120 min irradiation, whereas the oxidation efficiency was enhanced to 62.0% under oxic condition. Results of the photooxidation kinetics of As(III) over concentration range of 5–800 μM in the presence of CHO are provided in Fig. S9. $r_{As(III)}$ at different initial As(III) concentrations in the presence of 200 μM Cu(II) at pH 10 were collected for analysis by Langmuir-Hinshelwood (L-H) equation (Eq. (1)):

$$r_{As(III)} = \frac{k_{LH} K [As(III)]}{1 + K [As(III)]} \quad (1)$$

where k_{LH} the reaction rate; K the Langmuir adsorption constant. The kinetic curve fits well with the Langmuir-Hinshelwood model, indicating the interaction between As(III) and Cu(II) on CHO surface. Moreover, over the range of low concentration of As(III), the apparent kinetics can be simplified as pseudo-first order (inset of Fig. S9). Thus, the observed rate constants (k_{obs}) of As(III) oxidation were determined in terms of pseudo-first-order model (inset figure of Fig. 3a). The observed k_{obs} under anoxic conditions ($k_{obs,\ N2}$ = 0.0063 min^{-1}) was lower than that under oxic conditions ($k_{obs,\ Air}$ = 0.0086 min^{-1}), suggesting that oxygen can enhance the As(III) photooxidation. As shown in Fig. 3b, most of Cu(II) were retained under both oxic and anoxic conditions, which ruled out the adverse effect of the slight decrease of Cu(II) concentration on As(III) oxidation. The oxic conditions led to a slower accumulation of Cu(I) relative to anoxic conditions. Thus, the enhanced As(III) oxidation by oxygen might be due to the formation of less Cu(I), which compete for the light quanta with Cu(II) [53]. Oxygen enhanced 26.4% of the overall As(III) oxidation under oxic condition. Accordingly, oxygen was not a necessary but an enhancing factor for As(III) photooxidation.

If the LMCT process was the dominant way for As(III) oxidation in the presence of CHO, the direct electron transfer from As(III) to Cu(II) should lead to the production of As(V) and Cu(I). Thus, the observation of Cu(I) would support the LMCT process. Fig. 3b shows the generation of Cu(I) with the As(III) photooxidation to As(V) under oxic or anoxic conditions, suggesting the possible relationship between the reduction of Cu(II) and oxidation of As(III) (i.e. direct electron transfer). The stoichiometric ratio of Cu(I) to As(V) concentrations was approximately 2.0 in anoxic solutions with N_2 bubbling (inset figure of Fig. 3b). It was obviously to conclude that the successive a two-electron transfer from one As(III) to two Cu(II) occurred under anoxic conditions. While under

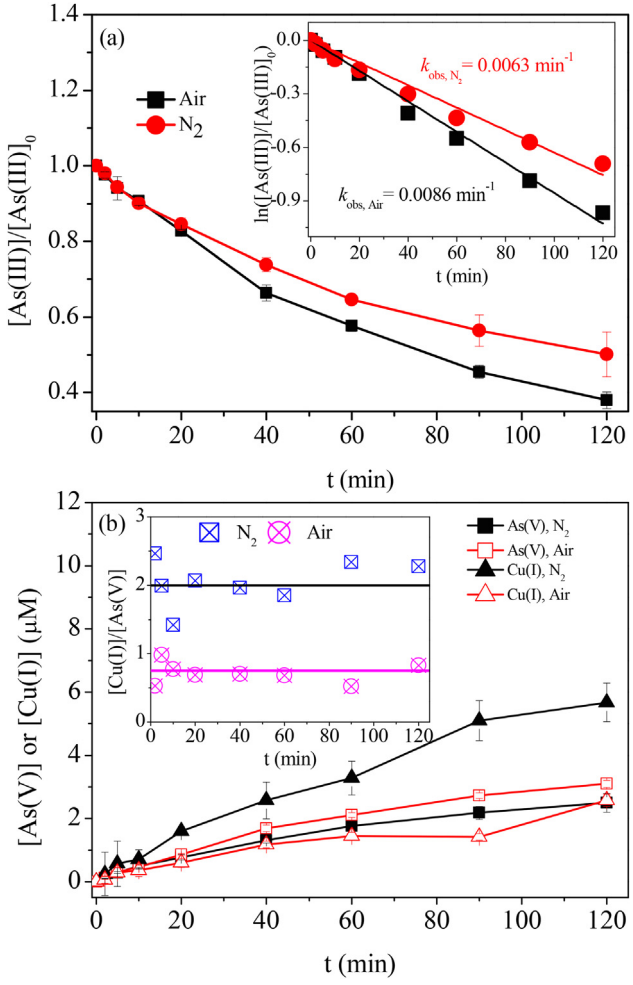

Fig. 3. (a) As(III) photooxidation and (b) Variations in the concentrations of As (V) and Cu(I) during As(III) photooxidation in CHO systems under oxic or anoxic conditions. The inset figure of (a): the observed rate constants (k_{obs}) using pseudo-first-order model; the inset figure of (b): the molar ratios of [Cu(I)] to [As(V)]. Experimental conditions: [Cu(II)] = 200 μM, [As(III)] = 5, pH 10, T = 25 °C.

oxic condition, only one electron transferred from As(III) to Cu(II), and the produced As(IV) was completed oxidized by O_2 rather than Cu(II) due to large rate constant for the reaction between As(IV) and O_2 ($k_{As(IV)/O2}$ = 1.4 × 10^9 M^{-1} s^{-1} at room temperature [54] and higher concentration of dissolved oxygen (ca. 0.3 mM, 1.5-fold of Cu(II)). Accordingly, the maximum [Cu(I)]/[As(V)] ratio under oxic conditions could be 1 if the produced Cu(I) was not oxidized by O_2 therein [55]. The experimental [Cu(I)]/[As(V)] ratio was ca. 0.75, indicating that ca. 25% produced Cu(I) was re-oxidized by O_2 simultaneously with As(III) oxidation. Similarly, the photographs of the reaction solutions are presented in Fig. S10. Without irradiation, clear solution (Fig. S10a) was changed to the green one (Fig. S10b) after 2 h stirring. Under anoxic conditions, the generated Cu(I) occurred in the form of Cu_2O particles with the brown color (Fig. S10c), whereas the less color and turbidity of the suspended solution was observed under oxic conditions (Fig. S10d).

Based on the discussion above, the photooxidation processes of As (III) on CHO surface include surface complexation and subsequent LMCT processes (Scheme 1). Under alkaline condition, the soluble As (III) oxyanion is adsorbed on CHO surface (expressed as >) to form the Cu(II)–As(III) complex (reactions (2) and (3)). Subsequently, light induces an electron transfer from As(III) to Cu(II) within the complex, resulting in As(III) oxidation to As(IV) and Cu(II) reduction to Cu(I) simultaneously (reactions (4)). Finally, the intermediate As(IV) was rapidly oxidized by Cu(II) in the absence of oxygen (reaction (5)) or by O_2 (reactions (6) and (7)) [50] along with the generation of Cu(II)–As (V) precipitates.

$$> Cu^{II}(OH)_2 + As^{III}O(OH)_2^- \rightarrow > Cu^{II}(OH)OAs^{III}(OH)_2 + OH^- \quad (2)$$

$$> Cu^{II}(OH)OAs^{III}(OH)_2 \rightarrow > Cu^{II}O_2As^{III}OH + H_2O \quad (3)$$

$$> Cu^{II}O_2As^{III}OH + h\nu + OH^- \rightarrow [> Cu^{I}O_2As^{IV}(OH)_2]^- \quad (4)$$

$$[> Cu^{I}O_2As^{IV}(OH)_2]^- + > Cu^{II}(OH)_2 \rightarrow [> Cu^{I}O_2As^{V}(O)OH]^- + > Cu^{I}OH + H_2O \quad (5)$$

$$[> Cu^{I}O_2As^{IV}(OH)_2]^- + O_2 \rightarrow [> Cu^{I}O_2As^{V}(O)OH]^- + O_2^{\cdot -} + H^+ \quad (6)$$

$$[> Cu^{I}O_2As^{V}(O)OH]^- + O_2 \rightarrow > Cu^{II}O_2As^{V}(O)OH + O_2^{\cdot -} \quad (7)$$

3.4. Effect of irradiation energy on the initial rate of As(III) oxidation

In this study, As(III) was oxidized to As(V) under a relative alkaline conditions (pH > 8) when irradiated by simulated solar radiation, while negligible oxidation of As(III) was observed in dark (Fig. 1a), suggesting the importance of light for As(III) oxidation at earth's surface environments. Fig. 4 presented a linear relation between $r_{As(III)}$ and irradiation intensity with a slope of 0.20 ± 0.02. Thus the quantum yield for the production of As(V) at 365 nm ($\Phi_{As(V),365nm}$) was calculated as (2.3 ± 0.2) × 10^{-2}, following the same order of magnitude as Cu(II)–maleate complex ($\Phi_{Cu(I),313nm}$ = (0.8 ± 0.2) × 10^{-2}) [39], and Cu(II)–iminodiacetic acid complex ($\Phi_{Cu(I),254nm}$ = 1.2 × 10^{-2}) [42] (Detailed description of the quantum yield calculation is provided in Text S4). Therefore, appropriately up-regulating the irradiation intensity was a suitable method to accelerate As(III) oxidation.

3.5. Formation of Cu(II)–As(III) complex

Fig. S11 shows that the CHO particle size increased over time in 1 h at pH 10. The peak of the particle size of CHO after 60 min agitation was extended by As(III) addition from the mean value of 670 nm (410–1100 nm) to 760 nm (470–1250 nm). In dark, dissolved As(III) concentration in the presence of CHO decreased sharply in first 10 min due to the formation of light green precipitate (Figs. S12 and S13). These results are consistent with As(III) adsorption on copper(II) oxides [24,26].

In LMCT process, an electron should be transferred from the ligand to metal, and a charge-transfer spectrum of complexes should be observed in UV–vis spectroscopy [56]. The UV–vis absorption spectra of As(III), Cu(II), and Cu(II)–As(III) complex were collected at pH 10 at various [Cu(II)]/[As(III)] ratios (Fig. S14). 10 μM of Cu(II) alone exhibited UV adsorption at 200–450 nm. The addition of As(III) up to 300 μM led to an enhancement in the UV absorption with a gradual shift of the maximum absorbance from < 200 nm to 214.5 nm without the appearance of any isosbestic points (inset figure of Fig. S14), whereas As(III) alone exhibited no obvious absorption at 200–450 nm. The variations of absorbance confirmed the complexation between As (III) and Cu(II) and the formation of more than one complexes under this specific condition.

The pH metric titration method [48,49] was applied to ascertain the formation constant of Cu(II)–As(III) complexes (Fig. S15a and b). The curve for Cu(II)–As(III) complex formation extended to a maximum $\bar{n}$ value (ca. 2.2) (Fig. 5a), suggesting that the complexes had 1:1 and 1:2 metal/ligand stoichiometry at least in solutions, which contained 1 mM Cu(II) and 4 mM As(III). However, the concentration of Cu(II) was 40-fold higher than that of As(III) in the photooxidation experiments. Thus, only the 1:1 Cu(II)–As(III) complex was considered with the formation constant of log K_{f1} = 6.0, close to that of the Cu(II)–OH

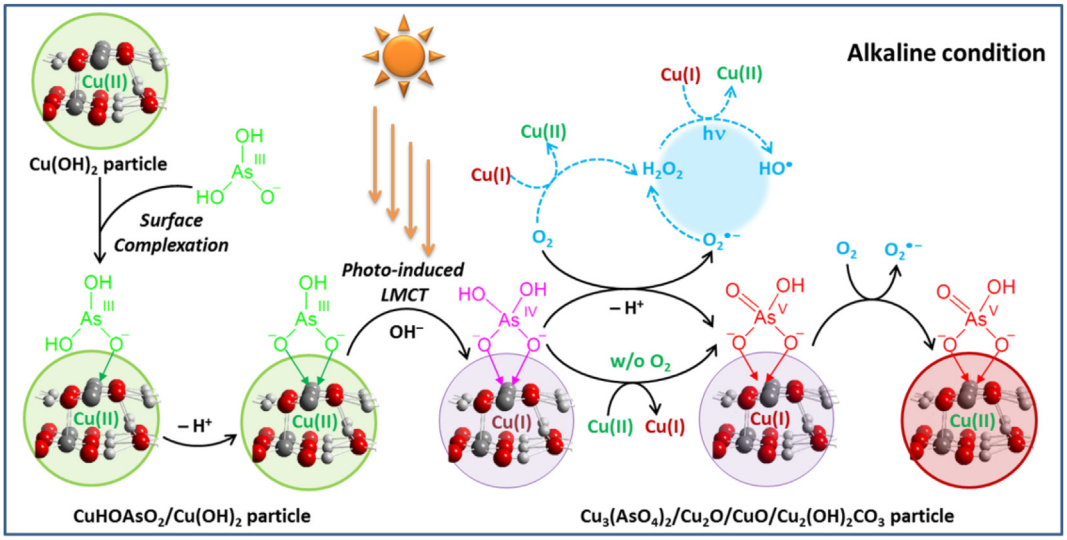

Scheme 1. Proposed photooxidation processes of As(III) by CHO through the formation of Cu(II)–As(III) complex under alkaline conditions in the presence of O_2.

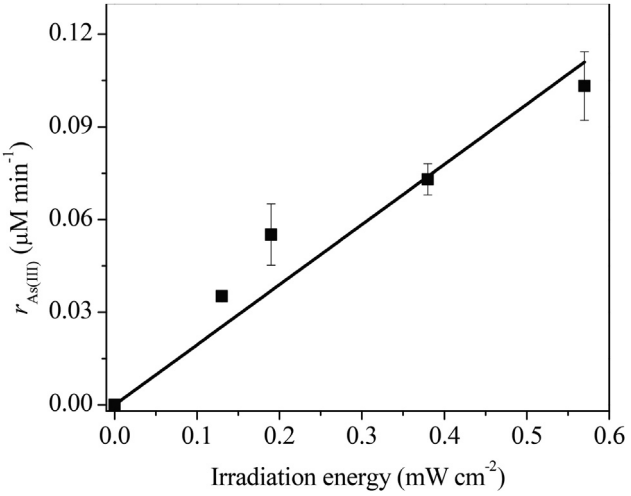

Fig. 4. Effect of irradiation energy on $r_{As(III)}$. The equation is $r_{As(III)}$ = (0.20 ± 0.02) × irradiation energy, R^2 = 0.97. Experimental conditions: [Cu(II)] = 200 μM, [As(III)] = 5 μM, pH 10, T = 25 °C.

complex (log K_1 = 7.0). The results revealed that the addition of As(III) could partially damage the structure of the Cu(II)–OH complex through forming Cu(II)–As(III) complexes, thereby resulting in an increase in the particle size of CHO (Fig. S11). Because As(III) oxidation via LMCT mostly depended on the formation of Cu(II)–As(III) complex on the nascent CHO particles, $r_{As(III)}$ could be simply expressed as Eq. (8).

$$r_{As(III)} = k_{Cu(II)-As(III)}[Cu(II)–As(III)] \quad (8)$$

Fig. 5b presented a significantly linear correlation between the $r_{As(III)}$ and the concentration of the Cu(II)–As(III) complex, confirming the dependence of As(III) oxidation on the complexation between Cu(II) and As(III). The best fit obtained the rate constant of $k_{Cu(II)-As(III)}$ = (6.7 ± 0.4) × 10^{-2} μM min^{-1} for the photolysis of Cu(II)–As(III) complex.

3.6. Characterization of the solid Cu(II)–As(III) complex

Solid Cu(II)–As(III) complex product was produced following the procedure described in "experimental section". The XRD pattern (Fig. S16) showed that the as-obtained sample had two broad peaks and some sharp peaks, revealing its good crystallinity with partial amorphous structure and big particle size. Compared with the XRD patterns of CuO (PDF#44-0706) and As_2O_3 (PDF#36-1490), the as-obtained sample produced some different sharp diffraction peaks at 2θ values of 22.8°, 33.4°, 35.7° and 52.6°, suggesting the formation of solid Cu(II)–As(III) complexes. Fig. S17a and b presented the XPS spectra of the $Cu2p_{3/2}$ and As3d, respectively. Fits of the $Cu2p_{3/2}$ spectra resulted in two sets of peaks at 933.5 eV and 935.2 eV for Cu(I)–O and Cu(II)–O, close to those at 933.0 eV and 935.1 eV, respectively, after As(III) adsorption and oxidation on the surface of CuO microspheres [29]. In the meantime, given the As(III) binding energies generally at approximately 1 eV lower than those of As(V) [28], the fitted curve for the As3d photoemission exhibited two sets of peaks at 44.4 eV and 45.4 eV for As(III)–O and As(V)–O, respectively. The latter one was close to that at 45.2 eV in Cu(II)–As(V) complex [26]. The mentioned higher binding energies for Cu(II)–O and As(III)–O in the as-obtained sample than those in CuO (933.5 eV) [57] and As_2O_3 (44.2 eV) [35] could be attributed to a higher degree of charge transfer from copper to arsenic, which confirmed the strong complexation between copper and arsenic. Although Cu(II) underwent reduction simultaneously with the oxidation of As(III), chemical analysis, determination of arsenic and copper species concentrations by dissolving the as-obtained sample in the HCl (1:1 v/v) solution, presented As(III)/Cu(II) molar ratio of ~1.97 without observed As(V) and Cu(I). Thus, the molar ratio of Cu(I)/As(V) reached ~ 2.1 (0.55/(0.13 × 1.97)) based on the calculation of Cu(I)/Cu_{total} (ca. 0.55) and As(V)/As_{total} (ca. 0.13) with the peak area, confirming that two electrons were successively transferred from As(III) to Cu(II) within solid Cu(II)–As(III) complex under X-ray irradiation. Accordingly, the as-obtained sample was expected as solid Cu(II)–As(III) complex product with a ~1:2 metal/ligand stoichiometry, which underwent photolysis via LMCT under the high-energy X-ray irradiation.

3.7. Solar photooxidation of As(III) by CHO and photolysis of the solid Cu(II)–As(III) complex

Experiments were performed to verify the effect of real sunlight on As(III) oxidation by CHO and results are shown in Fig. 6a. Comparison to As(III) oxidation under UV-A light (0.2 mW cm^{-2}), a similar oxidation efficiency of As(III) (ca. 60%) was achieved in sunlight with higher intensities (146.9–171.6 mW cm^{-2}). Though the utilization of sunlight was inadequate, the result sufficiently confirmed the sunlight-driven photooxidation of As(III) by CHO under alkaline conditions.

The rates of As(III) oxidation decreased on the aged CHO, and further dropped within the solid Cu(II)–As(III) complex at pH 10 compared with that on the nascent CHO (Fig. 6b). The affinity of Cu(II) oxides for

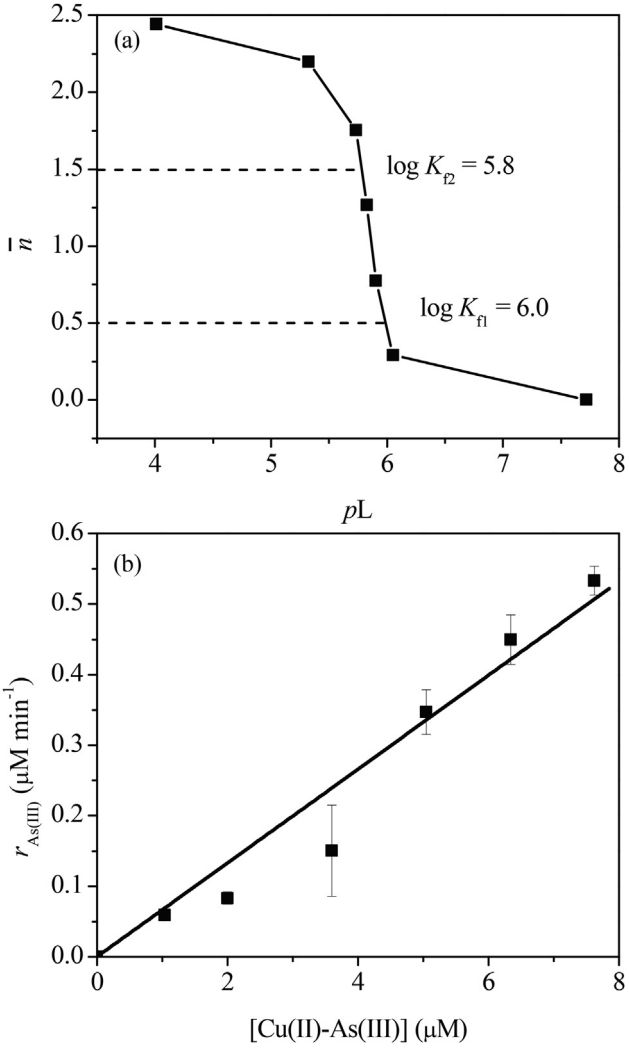

Fig. 5. (a) Formation curves of the Cu(II)–As(III) complex. Conditions: [As (III)] = 4 mM, [Cu(II)] = 1 mM, [$NaNO_3$] = 100 mM, [HNO_3] = 10 mM, $[NaOH]_{addition}$ = 213 mM, T = 25 °C. $\bar{n}$, the average number of ligands attached per metal ion, and *p*L, the exponent for free ligand. (b) Plot of the initial oxidation rates of As(III) ($r_{As(III)}$) versus [Cu(II)–As(III)]. Conditions: [Cu (II)] = 200 μM, [As(III)] = 5–50 μM, pH 10, T = 25 °C. The equation is written as $r_{As(III)} = (6.7 \pm 0.4) \times 10^{-2} \times$ [Cu(II)–As(III)], $R^2 = 0.98$.

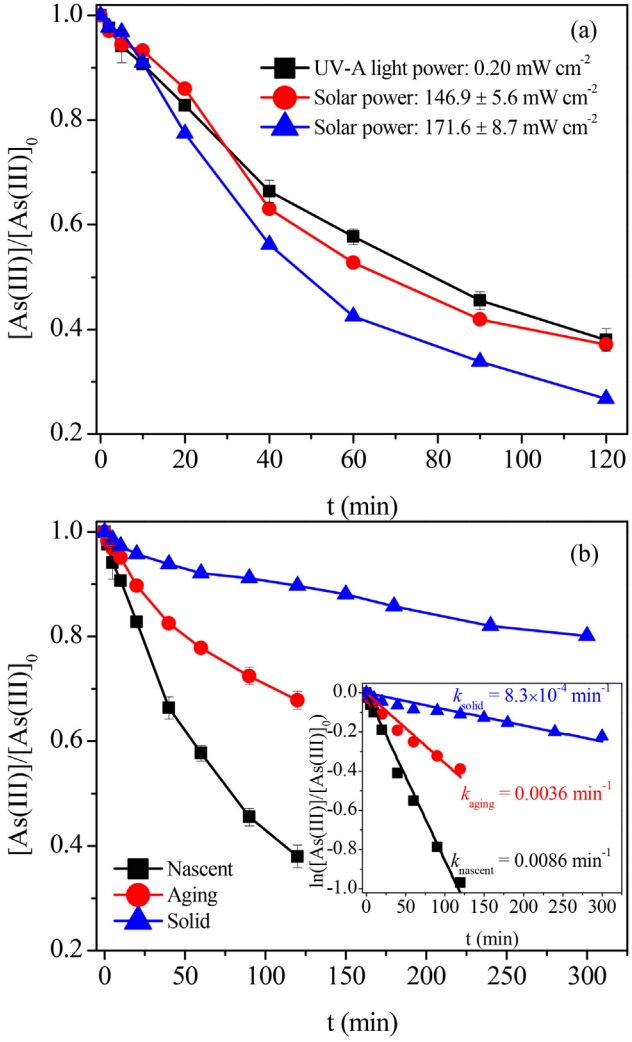

Fig. 6. (a) Effect of solar power on As(III) oxidation with nascent CHO; (b) Effect of aging on As(III) oxidation and the photolysis of solid Cu(II)–As(III) complex. Inset: (b) k_{obs} using pseudo-first-order model. Conditions: [Cu (II)] = 200 μM, [As(III)] = 5 μM, $[Cu(II)–As(III)]_{solid}$ = 10 mg L^{-1}, pH 10, T = 25 °C, ageing time = 2 h.

As(III) was obviously affected by the particle size of cupric oxides. In general, smaller particle size of Cu(II) oxides increased their sorption ability and reactivity for As(III) [24,26]. The nascent CHO was not stable under alkaline conditions. CHO nanoparticles grew gradually over time, and As(III) addition facilitated the particle growth with the formation of Cu(II)–As(III) complex (Figs. S11 and S13). Thus, nascent CHO with the smaller particle size facilitated As(III) complexation and photooxidation on CHO surface compared with the aged CHO and solid Cu(II)–As(III) complex. Although the observed oxidation rate constants of As(III) under sunlight or in the solid Cu(II)–As(III) complex were less than that under UV-A light in the presence of nascent CHO, they sufficiently confirmed the light-induced photooxidation of As(III).

4. Conclusion

This study manifested a novel photochemical reaction system, where the alleviation of water contamination from arsenic and copper was simultaneously achieved. The alkalinity driven hydrolysis of Cu^{2+} ions producing nascent CHO, which was applied as nano-absorber and electron acceptor for As(III) removal under irradiation. The final photoproduct can be easily recycled from the polluted water as stabilized Cu(II)–As(V) complex and precipitate. The mechanism study revealed that As(III) removal underwent a complexation-oxidation process. The adsorbed As(III) on CHO quickly formed surface Cu(II)–As(III) complex with a complexation constant of logK_{f1} = 6.0, and As(III) underwent photooxidation along with the reduction of Cu(II) to Cu(I) in the LMCT band with an As(V) production quantum yield of $(2.3 \pm 0.2) \times 10^{-2}$. The light-induced oxidation of As(III) in the presence of nascent CHO was independent of oxygen. The photooxidation of As(III) on aged CHO and within the solid Cu(II)–As(III) complex also occurred through the LMCT process. In short, the complexation between As(III) and Cu(II) as well as intramolecular electrons transfer within the complex present an overlooked mechanism of the photooxidative transformation of As(III) to As(V) under anoxic condition, especially in cases in which nascent CHO forms. This process could be potentially applied in technologies for arsenic recovery from copper-arsenic-containing environments.

Declaration of Competing Interest

The authors declare that they have no known competing financial interests or personal relationships that could have appeared to

influence the work reported in this paper.

Acknowledgments

This study was financed by National Natural Science Foundation of China (No. 21777125 and U1701241), National Postdoctoral Program for Innovative Talents (BX20190047), China Postdoctoral Science Foundation (2019M653340), and the Opening Fund of the State Key Laboratory of Environmental Geochemistry (SKLEG2019720).

Appendix A. Supplementary data

Supplementary data to this article can be found online at https://doi.org/10.1016/j.cej.2020.126102.

References

[1] Z. Yuan, G. Zhang, X. Ma, L. Yu, X. Wang, S. Wang, Y. Jia, Rapid abiotic As removal from As-rich acid mine drainage: effect of pH, Fe/As molar ratio, oxygen, temperature, initial As concentration and neutralization reagent, Chem. Eng. J. 378 (2019) 122156.
[2] C. Shan, H. Dong, P. Huang, M. Hua, Y. Liu, G. Gao, W. Zhang, L. Lv, B. Pan, Dual-functional millisphere of anion-exchanger-supported nanoceria for synergistic As (III) removal with stoichiometric H_2O_2: Catalytic oxidation and sorption, Chem. Eng. J. 360 (2019) 982–989.
[3] Z. Liu, H. Lei, T. Bai, W. Wang, K. Chen, J. Chen, Q. Hu, Microwave-assisted arsenic removal and the magnetic effects of typical arsenopyrite-bearing mine tailings, Chem. Eng. J. 272 (2015) 1–11.
[4] W. Ding, X. Huang, W. Zhang, F. Wu, J. Li, Sulfite activation by a low-leaching silica-supported copper catalyst for oxidation of As(III) in water at circumneutral pH, Chem. Eng. J. 359 (2019) 1518–1526.
[5] A. Wang, K. Zhou, X. Zhang, D. Zhou, C. Peng, W. Chen, Reductive removal of arsenic from waste acid containing high-acidity and arsenic levels through iodide and copper powder synergy, Chem. Eng. J. 373 (2019) 23–30.
[6] L. Chai, M. Yue, J. Yang, Q. Wang, Q. Li, H. Liu, Formation of tooeleite and the role of direct removal of As(III) from high-arsenic acid wastewater, J. Hazard. Mater. 320 (2016) 620–627.
[7] T. Luo, J. Cui, S. Hu, Y. Huang, C. Jing, Arsenic removal and recovery from copper smelting wastewater using TiO_2, Environ. Sci. Technol. 44 (2010) 9094–9098.
[8] J. Liu, P. Wu, S. Li, M. Chen, W. Cai, D. Zou, N. Zhu, Z. Dang, Synergistic deep removal of As(III) and Cd(II) by a calcined multifunctional MgZnFe-CO_3 layered double hydroxide: photooxidation, precipitation and adsorption, Chemosphere 225 (2019) 115–125.
[9] C.F. Harvey, K.N. Ashfaque, W. Yu, A. Badruzzaman, M.A. Ali, P.M. Oates, H.A. Michael, R.B. Neumann, R. Beckie, S. Islam, M.F. Ahmed, Groundwater dynamics and arsenic contamination in Bangladesh, Chem. Geol. 228 (2006) 112–136.
[10] M. Chen, J. Liu, Y. Bi, S. Rehman, Z. Dang, P. Wu, Multifunctional magnetic MgMn-oxide composite for efficient purification of Cd^{2+} and paracetamol pollution: Synergetic effect and stability, J. Hazard. Mater. 388 (2020) 122078.
[11] S. Ou, J. Zheng, G. Kong, C. Wu, Designed synthesis of a series of zwitterion–polyoxometalate hybrid materials for selective scavenging and photolysis of dyes, Dalton T. 44 (2015) 7862–7869.
[12] K. Im, D. Kim, J. Jang, J. Kim, S.J. Yoo, Hollow-sphere Co-NC synthesis by incorporation of ultrasonic spray pyrolysis and pseudomorphic replication and its enhanced activity toward oxygen reduction reaction, Appl. Catal. B-Environ. 260 (2020) 118192.
[13] S. Yang, X. Duan, J. Liu, P. Wu, C. Li, X. Dong, N. Zhu, D.D. Dionysiou, Efficient peroxymonosulfate activation and bisphenol A degradation derived from mineral-carbon materials: key role of double mineral-templates, Appl. Catal. B-Environ. 267 (2020) 118701.
[14] S. Yang, P. Wu, J. Liu, M. Chen, Z. Ahmed, N. Zhu, Efficient removal of bisphenol A by superoxide radical and singlet oxygen generated from peroxymonosulfate activated with Fe^0-montmorillonite, Chem. Eng. J. 350 (2018) 484–495.
[15] Z. Huang, P. Wu, J. Liu, S. Yang, M. Chen, Y. Li, W. Niu, Q. Ye, Defect-rich carbon based bimetallic oxides with abundant oxygen vacancies as highly active catalysts for enhanced 4-aminobenzoic acid ethyl ester (ABEE) degradation toward peroxymonosulfate activation, Chem. Eng. J. 395 (2020) 124936.
[16] J. Liu, P. Wu, S. Yang, S. Rehman, Z. Ahmed, N. Zhu, Z. Dang, Z. Liu, A photo-switch for peroxydisulfate non-radical/radical activation over layered CuFe oxide: Rational degradation pathway choice for pollutants, Appl. Catal. B-Environ. 261 (2020) 118232.
[17] J. Tucek, R. Prucek, J. Kolarik, G. Zoppellaro, M. Petr, J. Filip, V.K. Sharma, R. Zboril, Zero-valent iron nanoparticles reduce arsenites and arsenates to As(0) firmly embedded in core-shell superstructure: challenging strategy of arsenic treatment under anoxic conditions, ACS Sustain. Chem. Eng. 5 (2017) 3027–3038.
[18] D. Lakshmanan, D.A. Clifford, G. Samanta, Comparative study of arsenic removal by iron using electrocoagulation and chemical coagulation, Water Res. 44 (2010) 5641–5652.
[19] B.J. Watten, P.L. Sibrell, M.F. Schwartz, Acid neutralization within limestone sand reactors receiving coal mine drainage, Environ. Pollut. 137 (2005) 295–304.
[20] F.L. Pantuzzo, V.S.T. Ciminelli, Arsenic association and stability in long-term disposed arsenic residues, Water Res. 44 (2010) 5631–5640.
[21] L. Liu, W. Tan, S.L. Suib, G. Qiu, L. Zheng, S. Su, Enhanced adsorption removal of arsenic from mining wastewater using birnessite under electrochemical redox reactions, Chem. Eng. J. 375 (2019) 122051.
[22] J. Zeng, P. Qi, J. Shi, T. Pichler, F. Wang, Y. Wang, K. Sui, Chitosan functionalized iron nanosheet for enhanced removal of As(III) and Sb(III): Synergistic effect and mechanism, Chem. Eng. J. 382 (2020) 122999.
[23] A. Cao, J.D. Monnell, C. Matranga, J. Wu, L. Cao, D. Gao, Hierarchical nanostructured copper oxide and its application in arsenic removal, J. Phys. Chem. C. 111 (2007) 18624–18628.
[24] A. Goswami, P.K. Raul, M.K. Purkait, Arsenic adsorption using copper(II) oxide nanoparticles, Chem. Eng. Res. Des. 90 (2012) 1387–1396.
[25] J. Liu, B. Dhungana, G.P. Cobb, Environmental behavior, potential phytotoxicity, and accumulation of copper oxide nanoparticles and arsenic in rice plants, Environ. Toxicol. Chem. 37 (2018) 11–20.
[26] C.A. Martinson, K.J. Reddy, Adsorption of arsenic(III) and arsenic(V) by cupric oxide nanoparticles, J. Colloid Interf. Sci. 336 (2009) 406–411.
[27] K.J. Reddy, K.J. McDonald, H. King, A novel arsenic removal process for water using cupric oxide nanoparticles, J. Colloid Interf. Sci. 397 (2013) 96–102.
[28] K.J. McDonald, B. Reynolds, K.J. Reddy, Intrinsic properties of cupric oxide nanoparticles enable effective filtration of arsenic from water, Sci. Rep. 5 (2015) 11110–11119.
[29] X. Yu, R. Xu, C. Gao, T. Luo, Y. Jia, J. Liu, X. Huang, Novel 3D hierarchical cotton-candy-like CuO: surfactant-free solvothermal synthesis and application in As(III) removal, ACS Appl. Mater. Inter. 4 (2012) 1954–1962.
[30] J. Matschullat, Arsenic in the geosphere-a review, Sci. Total Environ. 249 (2000) 297–312.
[31] M. Chen, P. Wu, N. Zhu, Z. Dang, Y. Bi, F. Pei, Re-utilization of spent Cu2+-immobilized MgMn-layered double hydroxide for efficient sulfamethoxazole degradation: Performance and metals synergy, Chem. Eng. J. 392 (2020) 123709.
[32] A. Meharg, The arsenic green, Nature 423 (2003) 688.
[33] D. Fullston, D. Fornasiero, J. Ralston, Oxidation of synthetic and natural samples of enargite and tennantite: 2. X-ray photoelectron spectroscopic study, Langmuir 15 (1999) 4530–4536.
[34] M. Grafe, D.A. Beattie, E. Smith, W.M. Skinner, B. Singh, Copper and arsenate co-sorption at the mineral-water interfaces of goethite and jarosite, J. Colloid Interf. Sci. 322 (2008) 399–413.
[35] I.P. Pozdnyakov, W. Ding, J. Xu, L. Chen, F. Wu, V.P. Grivin, V.F. Plyusnin, Photochemical transformation of an iron(III)-arsenite complex in acidic aqueous solution, Photoch. Photobio. Sci. 15 (2016) 431–439.
[36] J. Xu, J.J. Li, F. Wu, Y. Zhang, Rapid photooxidation of As(III) through surface complexation with nascent colloidal ferric hydroxide, Environ. Sci. Technol. 48 (2014) 272–278.
[37] J. Sykora, Photochemistry of copper complexes and their environmental aspects, Coordin. Chem. Rev. 159 (1997) 95–108.
[38] F. Wu, N.S. Deng, Photochemistry of hydrolytic iron(III) species and photoinduced degradation of organic compounds. A minireview, Chemosphere 41 (2000) 1137–1147.
[39] L. Sun, C. Wu, B.C. Faust, Photochemical redox reactions of inner-sphere copper(II)-dicarboxylate complexes: Effects of the dicarboxylate ligand structure on copper(I) quantum yields, J. Phys. Chem. A 102 (1998) 8664–8672.
[40] C.H. Wu, L.Z. Sun, B.C. Faust, Photochemical formation of copper(I) from copper (II)-dicarboxylate complexes: effects of outer-sphere versus inner-sphere coordination and of quenching by malonate, J. Phys. Chem. A 104 (2000) 4989–4996.
[41] K. Hayase, R.G. Zepp, Photolysis of copper(II)-amino acid complexes in water, Environ. Sci. Technol. 25 (1991) 1273–1279.
[42] G. Mailhot, S.L. Andrianirinaharivelo, M. Bolte, Photochemical transformation of iminodiacetic acid induced by complexation with copper(II) in aqueous solution, J. Phys. Chem. A 87 (1995) 31–36.
[43] C.H. Langford, M. Wingham, V.S. Sastri, Ligand photooxidation in copper(II) complexes of nitrilotriacetic acid. Implications for natural waters, Environ. Sci. Technol. 7 (1973) 820–822.
[44] X. Wei, J. Chen, Q. Xie, S. Zhang, Y. Li, Y. Zhang, H. Xie, Photochemical behavior of antibiotics impacted by complexation effects of concomitant metals: a case for ciprofloxacin and Cu(II), Environ. Sci-Proc. Imp. 17 (2015) 1220–1227.
[45] W. Ding, J. Xu, T. Chen, C. Liu, J. Li, F. Wu, Co-oxidation of As(III) and Fe(II) by oxygen through complexation between As(III) and Fe(II)/Fe(III) species, Water Res. 143 (2018) 599–607.
[46] J.W. Moffett, R.G. Zika, R.G. Petasne, Evaluation of bathocuproine for the spectrophotometric determination of copper(I) in copper redox studies with applications in studies of natural-waters, Anal. Chim. Acta. 175 (1985) 171–179.
[47] Y.G. Zuo, Y.W. Deng, Evidence for the production of hydrogen peroxide in rainwater by lightning during thunderstorms, Geochim. Cosmochim. Acta. 63 (1999) 3451–3455.
[48] J. Bjerrum, Metal ammine formation in aqueous solution, P. Hasse and Sons, Copenhagen, 1941.
[49] H. Rossotti, H. Irving, The calculation of formation curves of metal complexes from pH titration curves in mixed solvents, J. Chem. Soc. 4 (1954) 2904–2910.
[50] A.N. Pham, G. Xing, C.J. Miller, T.D. Waite, Fenton-like copper redox chemistry revisited: hydrogen peroxide and superoxide mediation of copper-catalyzed oxidant production, J. Catal. 301 (2013) 54–64.
[51] S. Yoon, S. Jeong, S. Lee, Oxidation of bisphenol A by UV/$S_2O_8^{2-}$: comparison with UV/H_2O_2, Environ. Technol. 33 (2012) 123–128.
[52] X. Xiao, J. Xue, L. Liao, M. Huang, B. Zhou, B. He, A highly sensitive fluorescence probe for metallothioneins based on tiron−copper complex, Spectrochim. Acta. A.

145 (2015) 85–89.
[53] B. Wang, W. Zhang, Z. Zhang, R. Li, Y. Wu, Z. Hu, X. Wu, C. Guo, G. Cheng, R. Zheng, Cu_2O hollow structures-microstructural evolution and photocatalytic properties, RSC Adv. 6 (2016) 103700–103706.
[54] S. Yoon, J.H. Lee, S. Oh, J.E. Yang, Photochemical oxidation of As(III) by vacuum-UV lamp irradiation, Water Res. 42 (2008) 3455–3463.
[55] X. Yuan, A.N. Pham, C.J. Miller, T.D. Waite, Copper-catalyzed hydroquinone oxidation and associated redox cycling of copper under conditions typical of natural saline waters, Environ. Sci. Technol. 47 (2013) 8355–8364.
[56] A. Mostafa, N. El-Ghossein, G.B. Cieslinski, H.S. Bazzi, UV-Vis, IR spectra and thermal studies of charge transfer complexes formed in the reaction of 4-benzyl-piperidine with sigma- and pi-electron acceptors, J. Mol. Struct. 1054 (2013) 199–208.
[57] C. Wu, M. Yin, S. O'Brien, J.T. Koberstein, Quantitative analysis of copper oxide nanoparticle composition and structure by X-ray photoelectron spectroscopy, Chem. Mater. 18 (2006) 6054–6058.